Available online at www.sciencedirect.com

SciVerse ScienceDirect

Ceramics International 39 (2013) 5651–5658

CERAMICS INTERNATIONAL

www.elsevier.com/locate/ceramint

Polyvinylpyrrolidone (PVP)/$MnFe_2O_4$ nanocomposite: Sol–Gel autocombustion synthesis and its magnetic characterization

R. Topkaya[a], U. Kurtan[b,*], A. Baykal[b], M.S. Toprak[c,d]

[a]Department of Physics, Gebze Institute of Technology, 41400 Gebze-Kocaeli, Turkey
[b]Department of Chemistry, Fatih University, 34500 B.Çekmece-Istanbul, Turkey
[c]Department of Material sand Nanophysics, KTH-Royal Institute of Technology, 16440 Kista-Stockholm, Sweden
[d]Department of Materials Science and Engineering, Yildirim Beyazit University, Ulus-Ankara, Turkey

Received 17 December 2012; received in revised form 24 December 2012; accepted 24 December 2012
Available online 11 January 2013

Abstract

A polyvinylpyrrolidone (PVP)/$MnFe_2O_4$ nanocomposite was prepared by the sol–gel autocombustion method and its structural, thermal, spectroscoppic, morphological and magnetic characterizations were done by XRD, FT-IR, TGA, SEM and VSM techniques. The presence of $MnFe_2O_4$ was confirmed by XRD and the size of crystallites was estimated to be 11 ± 3 nm. Morphology analysis by SEM revealed spherical agglomerates of 15 nm. The magnetization curves confirm a superparamagnetic behavior with a blocking temperature of 287 K. The M_r/M_s value suggests the presence of uniaxial anisotropy in $MnFe_2O_4$ nanoparticles, instead of the expected cubic anisotropy according to the Stoner–Wohlfarth model. The effective magnetic anisotropy constant K_{eff} has been determined to be about 1.42×10^6 erg/cm^3 which is significantly higher than that of the bulk $MnFe_2O_4$. This suggests a strong magnetic coupling between magnetically ordered core spins and disordered surface spins of the nanoparticles in the nanocomposite.

Keywords: A. Sol–gel; Superparamagnetism; $MnFe_2O_4$; Magnetic nanomaterials

1. Introduction

Magnetic nanoparticles have attracted great attention in recent decades due to their wide potential applications in high-density magnetic recording [1], magnetic drug-delivery [2], magnetic resonance imaging (MRI) [3], etc. Magnetic nanoparticles have unusual properties like superparamagnetism, spin-glass-like behavior, and spin canting effect due to the large surface-to-volume ratio of the nanoparticles and they are required to have a superparamagnetic character at room temperature for many applications [4]. Among the known magnetic nanoparticles, $MnFe_2O_4$, a well known soft magnetic material, has relatively high surface area, saturation magnetization and excellent chemical stability [5,6] and has been widely applied in electronics, microwave devices, magnetic storage, etc. [7].

In order to prevent particle aggregation and control the average particle size and shape, a polar polymer, namely polyvinylpyrrolidone (PVP) can be extensively used as a reducing agent as well as a surface capping agent for the synthesis of nanoparticles [8]. PVP was often employed as a stabilizer in the preparation of composite spheres [9] and it has a well-defined structure with an N-vinylpyrrolidone monomer connected as a long chain. The incorporation of inorganic nanoparticles into a polymer matrix can result in significant improvements in a variety of chemical and physical properties [10–12].

In this work, a sol–gel auto-combustion method was used for the sysnthesis of PVP/$MnFe_2O_4$ nanocomposite. The structural, spectroscopic, thermal, morphological and magnetic properties of the PVP/$MnFe_2O_4$ nanocomposite

*Corresponding author. Tel.: +90 212 866330x2073; fax: +90 212 8663402.
E-mail address: ukurtan@fatih.edu.tr (U. Kurtan).

0272-8842/$ - see front matter © 2013 Elsevier Ltd and Techna Group S.r.l. All rights reserved.
http://dx.doi.org/10.1016/j.ceramint.2012.12.081

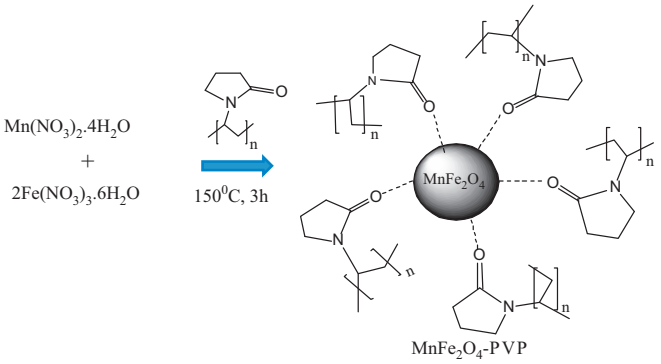

Scheme. The synthesis of PVP–$MnFe_2O_4$ nanocomposite.

have been investigated in details in the temperature range of 10–400 K and in magnetic fields up to 90 kOe.

2. Experimental

2.1. Chemicals and instrumentations

All chemicals including manganese nitrate hexahydrate ($Mn(NO_3)_2 \cdot 6H_2O$), iron nitrate nonahydrate ($Fe(NO_3)_3 \cdot 9H_2O$), citric acid ($C_6H_8O_7$), polyvinylpyrrolidone (PVP), ethylene glycol were obtained from Merck and used as received, without further purification.

X-ray powder diffraction (XRD) analysis was conducted on a Rigaku Smart Lab Diffractometer operated at 40 kV and 35 mA using Cu K_α radiation.

Fourier transform infrared (FT-IR) spectra were recorded in transmission mode (Perkin Elmer BX FT-IR) on powder samples that were ground with KBr and compressed into a pellet. FT-IR spectra in the range 4000–400 cm^{-1} were recorded in order to investigate the nature of the chemical bonds formed.

The thermal stability was determined by thermogravimetric analysis (TGA, Perkin Elmer Instruments model, STA 6000). The TGA thermograms were recorded for 5 mg of powder sample at a heating rate of 10 °C/min in the temperature range of 30–750 °C under nitrogen atmosphere.

Scanning Electron Microscopy (SEM) analysis was performed, in order to investigate the microstructure of the sample, using FEI XL40 Sirion FEG Digital Scanning Microscope. Samples were coated with gold at 10 mA for 2 min prior to SEM analysis.

The magnetization measurements were performed by using vibrating sample magnetometer (VSM, Quantum Design, PPMS 9 T) in an external field up to 90 kOe in the temperature range of 10–400 K. Field cooled (FC) and zero field cooled (ZFC) magnetization curves of the sample was measured at temperatures between 10 and 400 K with an applied magnetic field of 100 Oe. Firstly, the sample is cooled down from 400 to 10 K without any external magnetic field and then a magnetic field of 100 Oe is applied and ZFC data are recorded from 10 to 400 K. Secondly, the sample was cooled down again from 400 to 10 K in an applied field of 100 Oe and then the FC data were recorded from 10 to 400 K in the magnetic field of 100 Oe.

2.2. Procedure

PVP/$MnFe_2O_4$ nanocomposite was prepared by the sol–gel autocombustion method. An appropriate amount of $Mn(NO_3)_2 \cdot 6H_2O$ and $Fe(NO_3)_3 \cdot 6H_2O$ and citric acid ($C_6H_8O_7$) were first dissolved in a minimum amount of ethylene glycol. The molar ratio of nitrates was 1:2 and nitrates to citric acid were 1:1. Then a certain amount of polyvinylpyrrolidone (PVP) dissolved ethylene glycol was added into above metal nitrate solution. The final solution was magnetically stirred for 3 h at room temperature and then the water content was removed in an oven at 90 °C until a gel was obtained. The obtained gel in evaporating dish was dried in a hot air oven at 150 °C for about 5 h. Finally a black–brown color nanocomposite was obtained (Scheme).

3. Results and discussion

3.1. XRD analysis

The XRD pattern of PVP/$MnFe_2O_4$ nanocomposite is presented in Fig. 1. All of the observed diffraction peaks were indexed by the cubic structure of $MnFe_2O_4$ spinel (ICDD card no. 73-1964) phase. To determine the crystallite size of the product, its XRD profile was fitted according to the Eq. (1) in Wejrzanowski et al. [13] which allows the estimation of average crystallite size and its standard deviation from XRD. The experimental line profile, shown in Fig. 1 was fitted for 7 peaks (111), (220), (311), (400), (422), (511) and (440) [14–16]. The broadening of the diffraction peaks distinctly indicates the nanocrystalline nature of the materials. The average crystallite size of the product, D_{XRD}, determined to be 11 ± 3 nm.

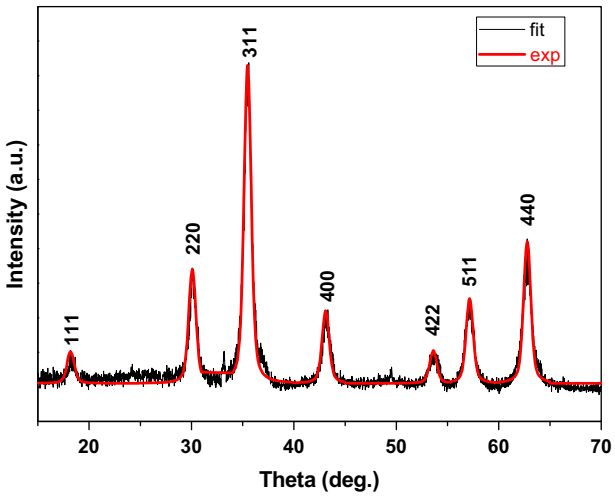

Fig. 1. XRD powder pattern of PVP/$MnFe_2O_4$ nanocomposite.

3.2. FT-IR analysis

The FT-IR spectra of PVP and PVP–$MnFe_2O_4$ nanocomposite are shown in Fig. 2. The C=O stretch band is present at 1663 cm^{-1} for pure PVP (Fig. 2(a)) and it appears at 1622 cm^{-1} for PVP/$MnFe_2O_4$ nanocomposite with ~41 cm^{-1} red shift. The asymmetric CH_2 stretch and symmetric CH_2 stretching were observed at 2922 cm^{-1} and 2852 cm^{-1}, respectively (Fig. 2b) [17,18]. The FT-IR spectra illustrate that absorption bands of Mn–O and Fe–O bonds appeared at 404, 502, and 556 cm^{-1}, respectively, for pure spinel manganese ferrite [19,20–22].

3.3. TG analysis

To further confirm the existence of PVP on the surface of $MnFe_2O_4$ nanoparticles and quantify the proportion of organic and inorganic phase, TG analysis was performed. Pure PVP combusted starting at 420 °C leaving a residue of ~8% above 450 °C (Fig. 3(a)). Evidently, the differential thermogram for the nanocomposite is slightly shifted toward higher temperatures due to the extra interaction between the PVP and nanoparticles [23–25]. Nanocomposite shows a major weight loss of 20% over the temperature range of 300–750 °C due to the decomposition and combustion of PVP (Fig. 3(b)). This implies that the nanocomposite has 80% inorganic phase as $MnFe_2O_4$ nanoparticles.

3.4. SEM analysis

Morphology of the nanocomposite was investigated by SEM and few micrographs at different magnifications are presented in Fig. 4. Spherical globules were observed that are heavily agglomerated. A closer inspection revealed the size of spheres are about 15 nm. This was in close agreement with the crystallite size estimated from X-ray line profile fitting, which may reveal nearly single crystalline character of the ferrite nanoparticles in the nanocomposite.

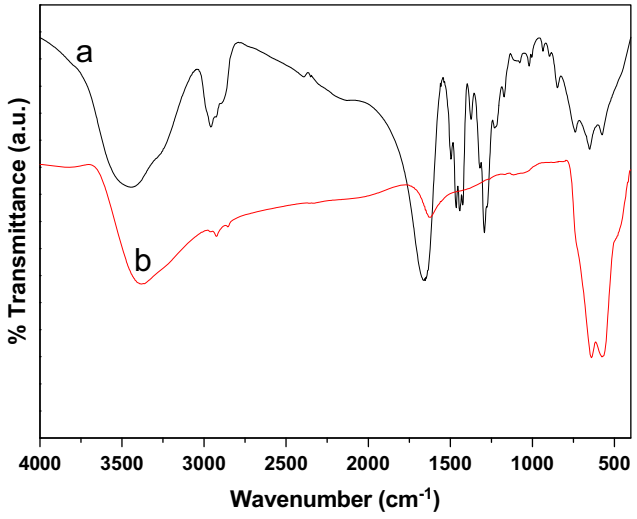

Fig. 2. FT-IR spectra of (a) PVP and (b) PVP/$MnFe_2O_4$ nanocomposite.

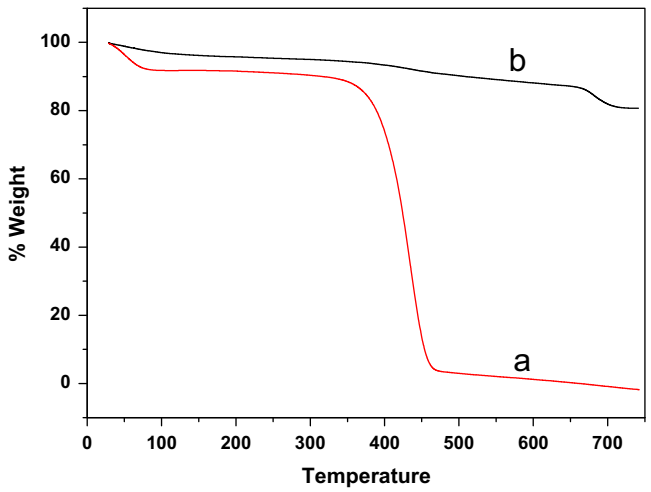

Fig. 3. TG thermographs of (a) PVP (b) PVP/$MnFe_2O_4$ nanocomposite.

3.5. VSM analysis

Field-dependent magnetization of the PVP/$MnFe_2O_4$ nanocomposite was measured in the temperature range of 10–300 K, and in magnetic fields ranging up to 60 kOe. Fig. 5 shows the field dependent magnetization curves taken at different temperatures for the PVP/$MnFe_2O_4$ nanocomposite between −1.5 kOe and +1.5 kOe. The sample shows hysteretic behavior at all temperatures except 300 K, where the coercivity and remanence are almost negligible, indicating that the $MnFe_2O_4$ nanoparticles in the nanocomposite exhibit superparamagnetic behavior at room temperature. It can be observed that the magnetization does not fully reach saturation even at magnetic fields as high as 90 kOe, suggesting the presence of antiferromagnetic interactions between ions of A and B sub lattices [26,27]. Similar results have been observed in the coated $Mn_xCo_{1-x}Fe_2O_4$ nanoparticles prepared by the glycothermal reaction [27] and $Mn_{0.2}Ni_{0.8}Fe_2O_4$ nanoparticles synthesized by a PEG-assisted hydrothermal route [28]. While the magnetization reaches to saturation by means of ferromagnetic contribution, it linearly increases due to antiferromagnetic contribution with the magnetic field. This results in unsaturated magnetization behavior [26].

Fig. 6 shows the variation of the saturation magnetization (M_s) values of the PVP/$MnFe_2O_4$ nanocomposite with temperature. The M_s values were determined by extrapolating M versus $1/H$ plot to $1/H=0$. As seen from the figure, as the temperature rises, the M_s values of the $MnFe_2O_4$ nanoparticles because of an increasing thermal fluctuations on magnetic ions as a function of temperature. The $MnFe_2O_4$ nanoparticles prepared by the sol–gel autocombustion method in this study have saturation magnetization of 40.4 and 52.1 emu/g at 300 and 10 K, respectively. The observed magnetization values are less

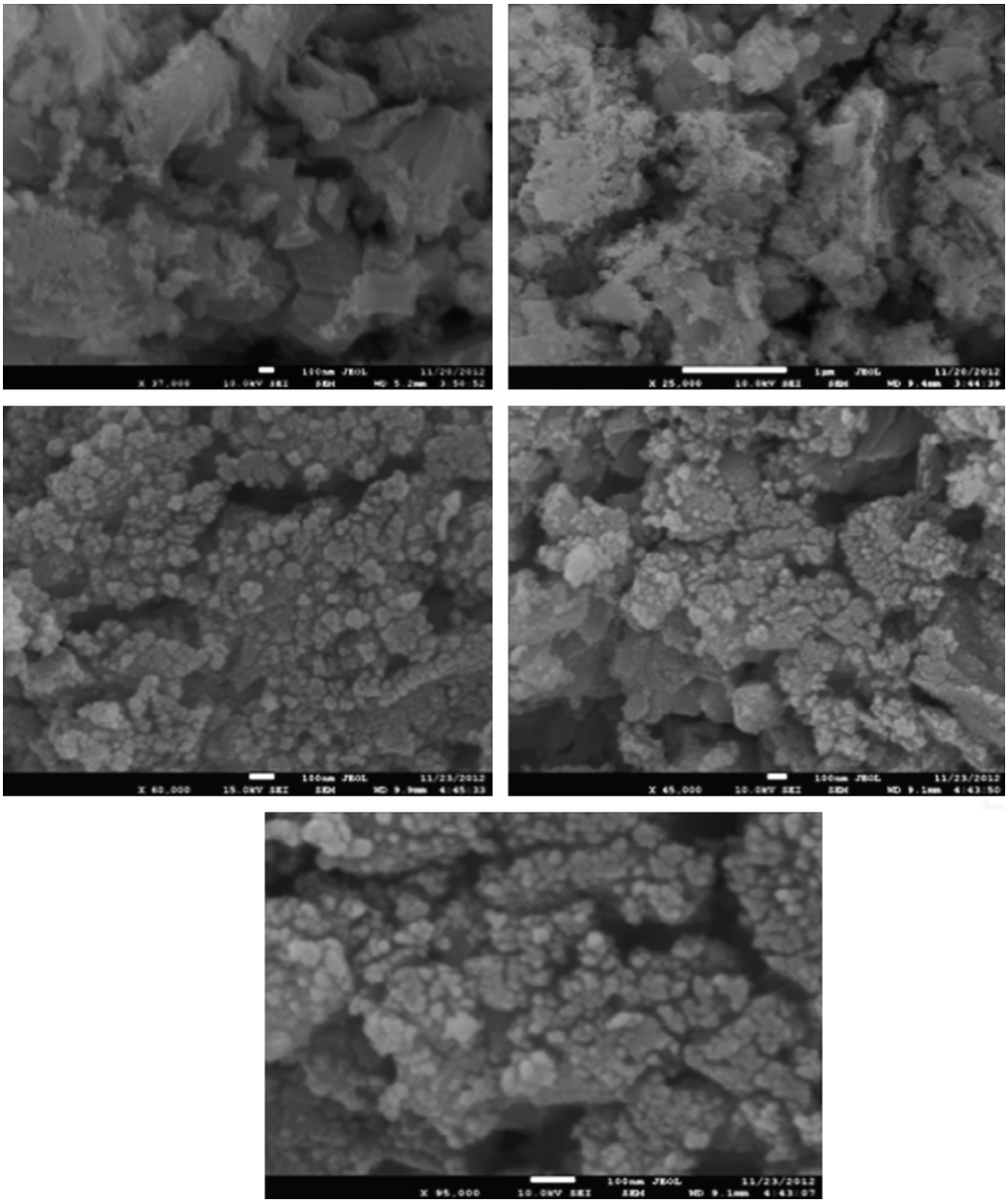

Fig. 4. SEM micrographs of PVP/$MnFe_2O_4$ nanocomposite with different magnifications.

than the value for bulk $MnFe_2O_4$ (80 emu/g) [29] and significantly higher than the values found for the $MnFe_2O_4$ nanoparticles of 15–23 nm synthesized by a thermal treatment method [30] and the $MnFe_2O_4$ nanoparticles of 12 nm prepared by reverse micelle microemulsion method [31]. It is known that the decrease in saturation magnetization of the nanoparticles is due to the surface spin disorder [32], spin canting occurring in nanoparticles [33], non-magnetic coating [34]. In this study, the reduction of saturation magnetization of the $MnFe_2O_4$ nanoparticles compared to that of the bulk can be ascribed to the non-magnetic PVP type polymer coating shell. Previous studies on magnetic nanoparticles have revealed that after non-magnetic coating, the saturation magnetization values decreases. For example, the M_s value of the magnetite nanoparticles synthesized through an oxidation–precipitation method decreases from 92 to 22.6 emu/g after poly(thiophene) coating [35]. The M_s value of the monodisperse cobalt ferrite nanomagnets decreases from 73.6 to 59.5 emu/g after silica coating [36]. The M_s Value of the $Zn_{0.6}Cu_{0.4}Cr_{0.5}Fe_{1.5}O_4$ nanocomposite prepared by a rheological phase reaction method from 28.3 to 5.9 emu/g after polyaniline (PANI) coating [37]. The PVP shell encapsulating on the surface of the nanoparticles and weakens magnetic dipole–dipole interactions between neighboring nanoparticles, which significantly decreases the saturation magnetization of the $MnFe_2O_4$ nanoparticles in this work.

Fig. 7 shows field cooled (FC) and zero field cooled (ZFC) magnetization curves of the PVP/$MnFe_2O_4$ nanocomposite measured at temperatures between 10 and

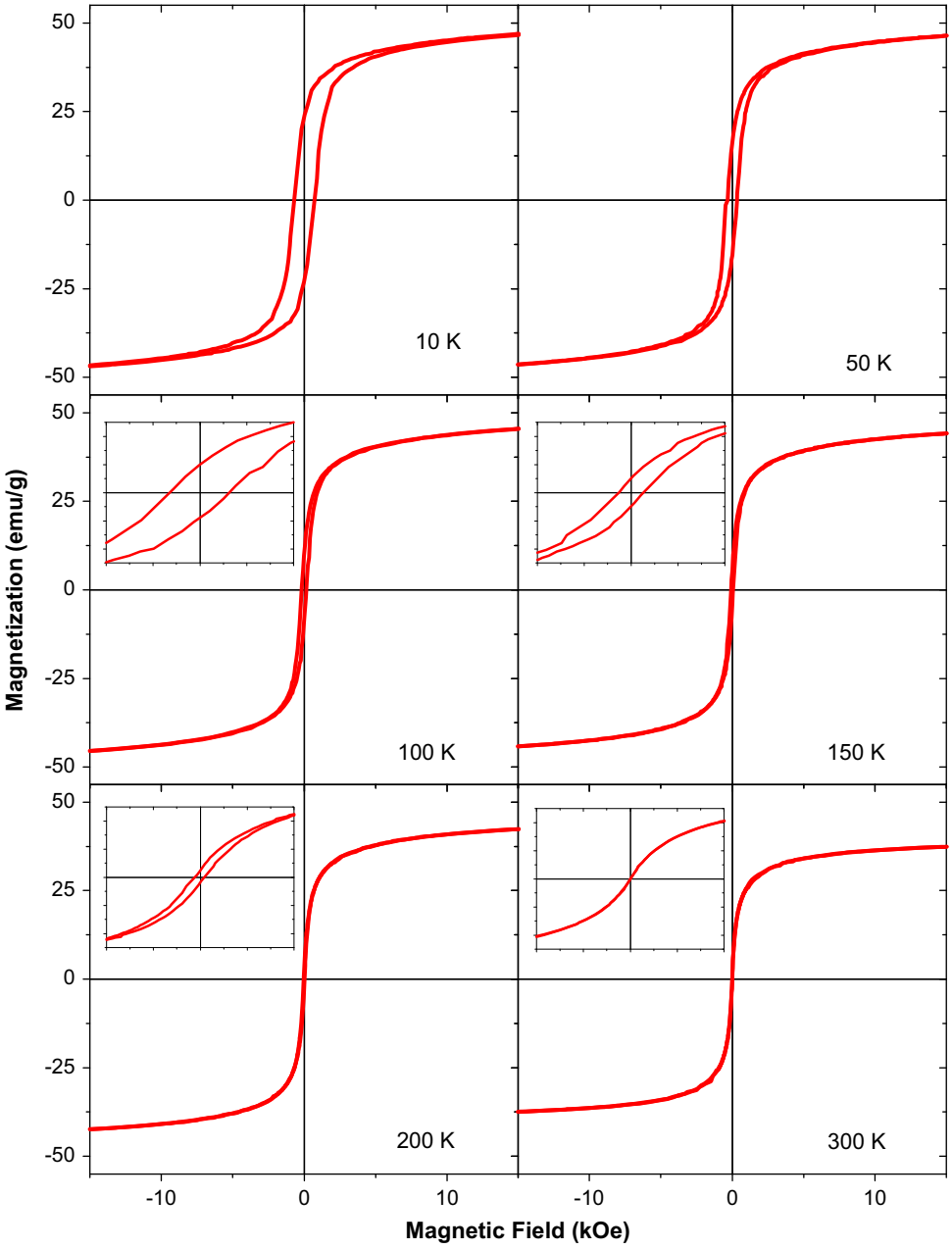

Fig. 5. Hysteresis loops of the PVP/$MnFe_2O_4$ nanocomposite measured at different temperatures.

400 K with an applied magnetic field of 100 Oe. The ZFC magnetization increases in the beginning as the temperature rises from 10 to 287 K. When the temperature is 287 K, it reaches a maximum and finally starts to decrease with increasing temperature. This particular temperature of 287 K at which the magnetization reaches a maximum is called the blocking temperature, T_B. Also, the FC curve remains almost constant below the blocking temperature. Such temperature dependence of the ZFC and FC magnetizations further confirms that the $MnFe_2O_4$ nanoparticles used in this work show superparamagnetic behavior at room temperature. At temperatures above T_B the thermal energy overcomes the anisotropy energy barrier and the direction of the magnetic moment of each nanoparticle randomly fluctuates from one easy direction to another. Thus, the magnetization decreases above T_B. This phenomenon is known as superparamagnetism [38]. It is also obvious that ZFC curve of the $MnFe_2O_4$ nanoparticles exhibits a broad peak at around T_B (287 K). This broad peak of ZFC curve is related with particle size distribution [39]. The broad peak observed in ZFC curve of the $MnFe_2O_4$ nanoparticles indicates broad size distribution of the particles used in this study.

Fig. 8 shows the thermal variation of the remanence magnetization for the PVP/$MnFe_2O_4$ nanocomposite. The inset of Fig. 8 shows the change in the reduced remanent magnetization (M_r/M_s) for the PVP/$MnFe_2O_4$ nanocomposite with temperature. It is observed from

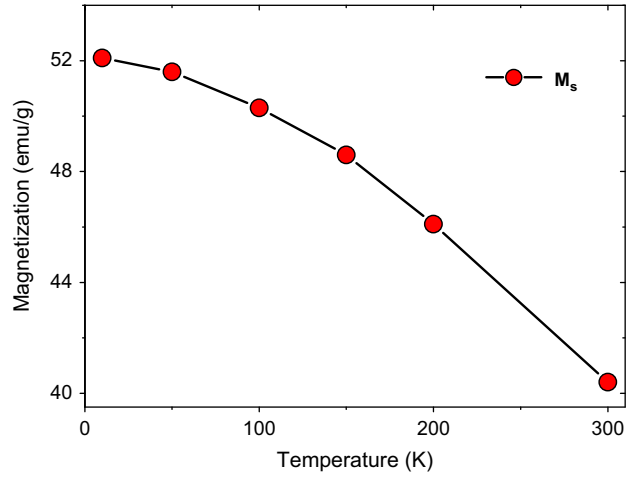

Fig. 6. Dependence of the saturation magnetization on temperature for the $MnFe_2O_4$ nanoparticles.

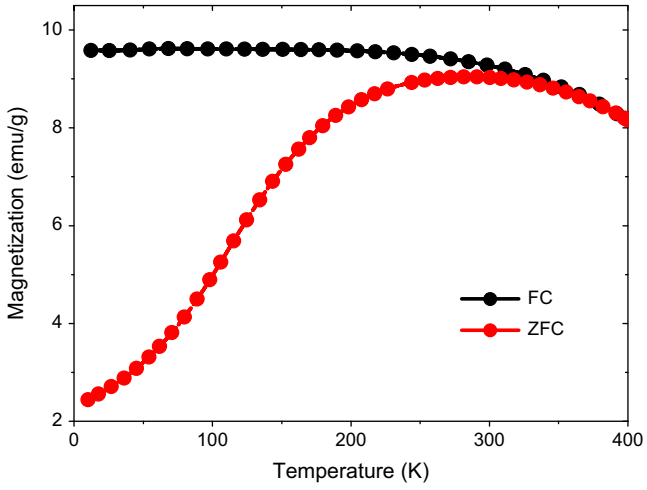

Fig. 7. ZFC–FC magnetization curves for the PVP/$MnFe_2O_4$ nanocomposite under an applied magnetic field of 100 Oe.

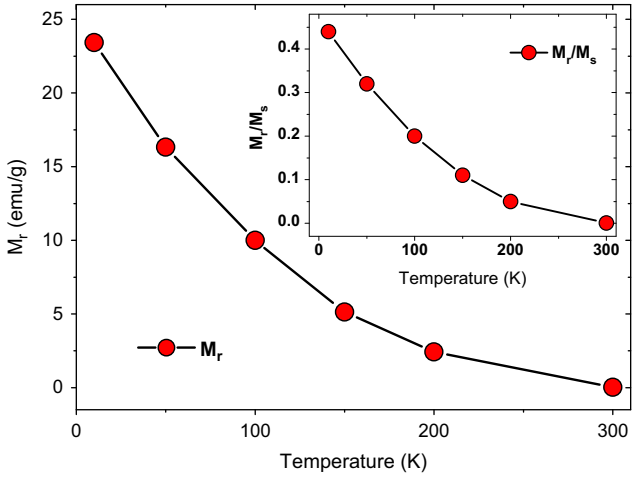

Fig. 8. Variation of the remanence magnetization, M_r with temperature of the PVP/$MnFe_2O_4$ nanocomposite. Inset shows variation of the reduced remanent magnetization (M_r/M_s) with temperature.

Fig. 8 that the M_r and M_r/M_s continuously decrease as the temperature increases. This behavior is due to the decrease of magnetic anisotropy strength with increasing temperature [40,41]. In the Stoner–Wohlfarth model for non-interacting single domain particles with the easy axis randomly oriented, the M_r/M_s is given by 0.5 for uniaxial anisotropy, and 0.832 for cubic anisotropy [42]. As seen from the inset of Fig. 8, at all temperatures the M_r/M_s value of the sample used in this study does not exceed the theoretical value of 0.5. The bulk $MnFe_2O_4$ is a magnetic material with cubic magnetocrystalline anisotropy [43]. However, according to the Stoner–Wohlfarth model, these M_r/M_s values are more consistent with uniaxial anisotropy instead of the expected cubic anisotropy. Thus, the $MnFe_2O_4$ nanoparticles used in this study have uniaxial anisotropy. Similar results have also been reported for cobalt substituted ferrite nanoparticles synthesized using reverse micelles [44] and ultrafine cobalt ferrite particles synthesized by hydrolysis in a polyol medium [45]. The uniaxial anisotropy seen in the magnetic nanoparticles is attributed to surface effects [46].

Fig. 9 shows variation of the coercive field, H_c of the PVP/$MnFe_2O_4$ nanocomposite with temperature. The H_c significantly depends on temperature and continuously decreases with increasing temperature. This is due to the decreasing of the effective magnetic anisotropy with increasing temperature. At room temperature, the H_c of the $MnFe_2O_4$ nanoparticles is almost negligible, indicating the superparamagnetic behavior. The coercivity is known to be a measure of the strength of the magnetic field that is required to overcome the energy barrier connected with the magnetocrystalline anisotropy energy. The magnetic anisotropy energy (E_A) for non-interacting single-domain particle with uniaxial anisotropy is defined by the Stoner–Wohlfarth theory [47]:

$$E_A = KV\sin^2\theta \quad (1)$$

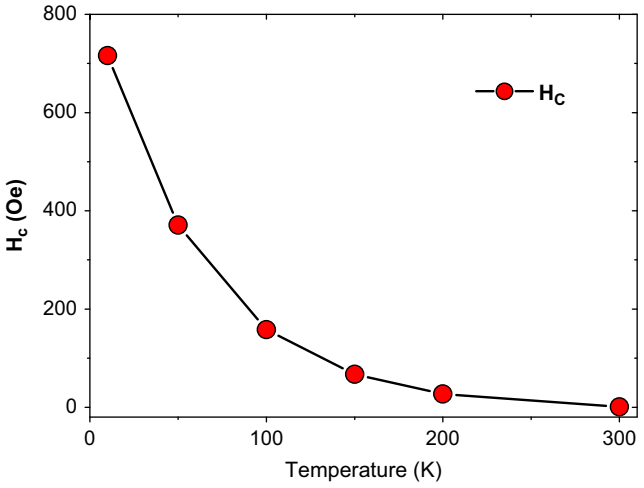

Fig. 9. The temperature dependence of the coercive field, H_c of the PVP/$MnFe_2O_4$ nanocomposite.

where K, V and θ are magnetic anisotropy energy constant and volume of the particles, and the angle between magnetization direction and the easy axis of a nanoparticle, respectively. The magnetic anisotropy energy barrier decreases as well as the magnetic anisotropy decreases, resulting in lower magnetic field strength for magnetization reversal (or lower H_c). The H_c value of the $MnFe_2O_4$ nanoparticles synthesized by the sol–gel autocombustion method in this study is 716; Oe at 10 K. Similar H_c values have also been observed for the nanosized $MnFe_2O_4$ ferrites synthesized by solid state ball- milling and calcinations of nitrate precursors and citric acid [47]. The magnetic anisotropy constant K_{eff} of the magnetite nanoparticles can be calculated using Eq. (2) give below [48];

$$K_{eff} V = 25 k_B T_B \quad (2)$$

Where V, k_B, T_B are the volume of a single particle, Boltzmann constant, and blocking temperature of the sample, respectively. The calculated magnetic anisotropy constant K_{eff} of the $MnFe_2O_4$ nanoparticles in this study is about 1.42×10^6 erg/cm^3 which is significantly higher than K_{eff} value of the bulk $MnFe_2O_4$ [43]. The surface spins of the magnetic nanoparticles affect the magnetic properties of the nanoparticles due to high surface to volume ratio of the nanoparticles [27]. The strong magnetic coupling occurring between magnetically ordered core spins and disordered surface spins of the nanoparticles with core-shell structure increases the effective magnetic anisotropy [49]. This can be the reason of large effective magnetic anisotropy observed in the $MnFe_2O_4$ nanoparticles prepared by the sol–gel autocombustion method in this study.

4. Conclusion

In this study, the synthesis and detailed characterization (using XRD, FT-IR, TGA, SEM and VSM techniques) of PVP/$MnFe_2O_4$ nanocomposite were presented. The crystalline phase was identified as $MnFe_2O_4$ and the size of crystallites was estimated as 11 ± 3 nm by X-ray line profile fitting. Morphology analysis by SEM revealed spherical agglomerates of 15 nm, which indicates nearly single crystalline character of nanoparticles in the composite. The hysteresis loop with almost negligible coercive field indicates a superparamagnetic behavior of the $MnFe_2O_4$ nanoparticles at room temperature. The ZFC–FC curves further confirm the superparamagnetic behavior with a blocking temperature T_B of 287 K. The M_s, H_c, M_r and M_r/M_s values decreases with increasing temperature. The observed M_r/M_s values lower than theoretical value of 0.5 indicate the $MnFe_2O_4$ nanoparticles, prepared by the sol–gel autocombustion method in this study, have uniaxial anisotropy rather than the expected cubic anisotropy according to the Stoner–Wohlfarth model. The calculated magnetic anisotropy constant K_{eff} of the $MnFe_2O_4$ nanoparticles in this study is about 1.42×10^6 erg/cm^3 which is significantly higher than that of the bulk $MnFe_2O_4$. This higher anisotropy is attributed to the strong magnetic coupling occurring between magnetically ordered core spins and disordered surface spins of the nanoparticles. These materials may be promising candidates for applications and the devised fabrication route is rather versatile that can be applied for the fabrication of other ferrite or oxide nanoparticle–nanocomposite systems.

Acknowledgment

This work is supported by the Fatih University under BAP Grant no. P50021104-B.

References

[1] T. Hayashi, S. Hirono, M. Tomita, S. Umemura, Magnetic thin films of cobalt nanocrystals encapsulated in graphite-like carbon, Nature 381 (1996) 772–774.
[2] I. Brigger, C. Dubernet, P. Couvreur, Nanoparticles in cancer therapy and diagnosis, Advanced Drug Delivery Reviews 54 (2002) 631–651.
[3] J.H. Lee, Y.M. Huh, Y.W. Jun, J.W. Seo, J.T. Jang, H.T. Song, S. Kim, E.J. Cho, H.G. Yoon, J.S. Suh, J. Cheon, Artificially engineered magnetic nanoparticles for ultra-sensitive molecular imaging, Nature Medicine 13 (2007) 95–99.
[4] P. Pradhan, J. Giri, G. Samanta, H.D. Sarma, K.P. Mishra, J.R. Bellare, R. Banerjee, D. Bahadur, Comparative evaluation of heating ability and biocompatibility of different ferrite based magnetic fluids for hyperthermia application, Journal of Biomedical Materials Research B 81B (2007) 12–22.
[5] R.C. Wu, J.H. Qu, Removal of water-soluble azo dye by the magnetic material $MnFe_2O_4$, Journal of Chemical Technology and Biotechnology 80 (2005) 20–27.
[6] L. Shao, Z. Ren, G. Zhang, L. Chen, Facile synthesis, characterization of a MnFe2O4/activated carbon magnetic composite and its effectiveness in tetracycline removalMater, Chemical Physics 135 (2012) 16–24.
[7] D. Chen, Y. Zhang, Z. Kang, A low temperature synthesis of MnFe2O4 nanocrystals by microwave-assisted ball-milling 215–216 (2013) 235–239Chemical Engineering Journal 215–216 (2013) 235–239.
[8] Z. Durmus, A. Baykal, H. Sozeri, M.S. Toprak, Preparation of PVP (Polyvinyl Pyrrolidone)/Ba–Sr hexaferrites via gel to crystalline method, synthesis and reactivity in ınorganic, Metal-Organic, and Nano-Metal Chemistry 42 (2012) 1390–1397.
[9] Y. Chi, Q. Yuan, Y. Li, J. Tu, L. Zhao, N. Lia, X. Li, Synthesis of Fe_3O_4@SiO_2–Ag magnetic nanocomposite based on small-sized and highly dispersed silver nanoparticles for catalytic reduction of 4-nitrophenol, Journal of Colloid and Interface Science 383 (2012) 96–102.
[10] T. Du, H. Song, O.J. Ilegbusi, Sol–gel derived ZnO/PVP nanocomposite thin film for superoxide radical sensor, Materials Science and Engineering: C 27 (2007) 414–420.
[11] O.J. Ilegbusi, H. Song, R. Chakrabarti, Sol–gel derived ZnO/PVP nanocomposite thin film for superoxide radical sensor, Journal of Bionic Engineering 7 (2010) 30–35.
[12] S. Ummartyotin, N. Bunnak, J. Juntaro, M. Sain, H. Manuspiya, Hybrid organic–inorganic of ZnS embedded PVP nanocomposite film for photoluminescent application, Comptes Rendus Physique 13 (2012) 994–1000.
[13] T. Wejrzanowski, R. Pielaszek, A. Opalińska, H. Matysiak, W. Lojkowski, K.J. Kurzydlowski, Quantitative methods for nanopowders characterization, Applied Surface Science 253 (2006) 204–209.
[14] A. Baykal, M. Günay, M.S. Toprak, H. Sozeri, Effect of ionic liquids on the electrical and magnetic performance of polyaniline–nickel ferrite nanocomposite, Materials Research Bulletin 48 (2013) 378–382.

[15] D. Chen, Y. Zhang, Z. Kan, A low temperature synthesis of $MnFe_2O_4$ nanocrystals by microwave-assisted ball-milling, Chemical Engineering Journal 215 (2013) 235–239.
[16] L. Zhen, K. He, C.Y. Xu, W.Z. Shao, Synthesis and characterization of single-crystalline $MnFe_2O_4$ nanorods via a surfactant-free hydrothermal route, Journal of Magnetism and Magnetic Materials 320 (2008) 2672–2675.
[17] A. Baykal, N. Bıtrak, B. Ünal, H. Kavas, Z. Durmus, S. Özden, M.S. Toprak, Polyol synthesis of (polyvinylpyrrolidone) PVP–Mn_3O_4 nanocomposite, Journal of Alloys and Compounds 502 (2010) 199–205.
[18] M. Chen, H. Qu, J. Zhu, Z. Luo, A. Khasanov, A.S. Kucknoor, N. Haldolaarachchige, D.P. Young, S. Wei, Z. Guo, Magnetic electrospun fluorescent polyvinylpyrrolidone nanocomposite fibers, Polymer 53 (2012) 4501–4511.
[19] R. Udayabhaskar, R.V. Mangalaraja, D. Manikandan, V. Arjunan, B. Karthikeyan, Room temperature synthesis and optical studies on Ag and Au mixed nanocomposite polyvinylpyrrolidone polymer films 99 (2012) 69–73.
[20] S.S. Kalyan Kamal, P.K. Sahoo, L. Durai, P. Ghosal, M. Manivel Raja, S. Ram, Synthesis and surface modified hard magnetic properties in $Co_{0.5}Pt_{0.5}$ nanocrystallites from a rheological liquid precursor, Journal of Magnetism and Magnetic Materials 324 (2012) 3893–3898.
[21] M. Gunay, H. Erdemi, A. Baykal, H. Sözeri, M.S. Toprak Triethylene glycol stabilized $MnFe_2O_4$ nanoparticle: synthesis, magnetic and electrical characterization, Materials Research Bulletin, 10.1016/j.materresbull.2012.11.097, in press.
[22] H. Sozeri, U. Kurtan, R. Topkaya, A. Baykal, M.S. Toprak, Polyaniline (PANI)–$Co_{0.5}Mn_{0.5}Fe_2O_4$ nanocomposite: synthesis, characterization and magnetic properties evaluation, Ceramics International, 10.1016/j.ceramint.2012.12.009, in press.
[23] Y. Xiaotun, X. Lingge, N.S. Choon, C.S. Hardy, Magnetic and electrical properties of polypyrrole-coated γ-Fe_2O_3 nanocomposite particles, Nanotechnology 14 (2003) 624.
[24] Z.J. Zhang, X.Y. Chen, B.N. Wang, C.W. Shi, Hydrothermal synthesis and self-assembly of magnetite (Fe_3O_4) nanoparticles with the magnetic and electrochemical properties, Journal of Crystal Growth 310 (2008) 5453.
[25] M. Chen, H. Qu, J. Zhu, Z. Luo, A. Khasanov, A.S. Kucknoor, N. Haldolaarachchige, D.P. Young, S. Wei, Z. Guo, Magnetic electrospun fluorescent polyvinylpyrrolidone nanocomposite fibers, Polymer 53 (2012) 4501–4511.
[26] K.K. Bharathi, R.J. Tackett, C.E. Botez, C.V. Ramana, Coexistence of spin glass behavior and long-range ferrimagnetic ordering in La- and Dy-doped Co ferrite, Journal of Applied Physics 109 (2011) 07A510.
[27] R. Topkaya, Ö. Akman, S. Kazan, B. Aktaş, Z. Durmus, A. Baykal, Surface spin disorder and spin-glass-like behaviour in manganese-substituted cobalt ferrite nanoparticles, Journal of Nanoparticle Research 14 (2012) 1156.
[28] Y. Köseoğlu, M. Bay, M. Tan, A. Baykal, H. Sözeri, R. Topkaya, N. Akdoğan, Magnetic and dielectric properties of $Mn_{0.2}Ni_{0.8}Fe_2O_4$ nanoparticles synthesized by PEG-assisted hydrothermal method, Journal of Nanoparticle Research 13 (2011) 2235–2244.
[29] V.A.M. Brabers, Progress in spinel ferrite research, in: K.H.J. Buschow (Ed.), Handbook of Magnetic Materials, vol. 8, Elsevier, New York, NY, USA, 1995 Chapter 3, pp. 189–324.
[30] M.G. Naseri, E.B. Saion, A. Kamali, International Scholarly Research Network ISRN Nanotechnology, 2012, Article ID 604241, 11 pp., 10.5402/2012/60424.
[31] C.R. Vestal, Z.J. Zhang, Synthesis and magnetic characterization of Mn and Co spinel ferrite–silica nanoparticles with tunable magnetic core, Nano Letters 3 (2003) 1739–1743.
[32] R.H. Kodama, A.E. Berkowitz, E.J. McNiff Jr., S. Foner, Surface spin disorder in $NiFe_2O_4$ naoparticles, Physical Review Letters 77 (1996) 394–397.
[33] J.M.D. Coey, Noncollinear spin arrangement in ultrafine ferrimagnetic crystallites, Physical Review Letters 27 (1971) 1140–1142.
[34] C. Chang, L. Zhao, M.K. Wu, Magnetodielectric study in SiO_2-coated Fe_3O_4 nanoparticle compacts, Journal of Applied Physics 108 (2010) 094105.
[35] L.F. Cótica, I.A. Santos, E.M. Girotto, E.V. Ferri, A.A. Coelho, Surface spin disorder effects in magnetite and poly(thiophene)-coated magnetite nanoparticles, Journal of Applied Physics 108 (2010) 064325.
[36] Q. Dai, M. Lam, S. Swanson, R.H.R. Yu, D.J. Milliron, T. Topuria, P.O. Jubert, A. Nelson, Monodisperse Cobalt Ferrite Nanomagnets with Uniform Silica Coatings, Langmuir 26 (2010) 17546–17551.
[37] J. Jiang, L. Li, M. Zhu, Polyaniline/magnetite ferrite nanocomposites obtained by in situ polymerization, Reactive & Functional Polymers 68 (2008) 57–62.
[38] A. Herpin, Theory of Magnetism, 1st ed., National Institute of Science and Nuclear Techniques, Saclay, 1968.
[39] P. Poddar, H. Srikanth, S.A. Morrison, E.E. Carpenter, Interparticle interactions and magnetism in manganese–zinc ferrite nanoparticles, Journal of Magnetism and Magnetic Materials 288 (2005) 443–451.
[40] N.D. Chaudhari, R.C. Kambale, D.N. Bhosale, S.S. Suryavanshi, S.R. Sawant, Thermal hysteresis and domain states in Ni–Zn ferrites synthesized by oxalate precursor method, Journal of Magnetism and Magnetic Materials 322 (2010) 1999–2005.
[41] J.H. Fendler, Y. Tian, Nanoparticles and nanostructured films: current accomplishments and future prospects, in: J.H. Fendler (Ed.), Nanoparticles and Nanostructured Films: Preparation, Characterization and Applications, Wiley-VCH Verlag GmbH, Weinheim, Germany, 2007 (Chapter 18), 10.1002/9783527612079.
[42] E.C. Stoner, E.P. Wohlfarth, A mechanism of magnetic hysteresis in heterogeneous alloys, Philosophical Transactions of the Royal Society A 240 (826) (1948) 599–642.
[43] B.D. Cullity, Introduction to Magnetic Materials, Addison-Wesley Pub. Co., Reading, MA, 1972.
[44] L. Victoria, C. DdelC, C. Rinaldi, Synthesis and magnetic characterization of cobalt-substituted ferrite ($Co_xFe_{3-x}O_4$) nanoparticles, Journal of Magnetism and Magnetic Materials 314 (2007) 60–67.
[45] S. Ammar, A. Helfen, N. Jouini, F. Fiévet, I. Rosenman, F. Villain, P. Molinié, M. Danot, Journal of Materials Chemistry 11 (2001) 186–192.
[46] R.H. Kodama, Magnetic nanoparticles, Journal of Magnetism and Magnetic Materials 200 (1–3) (1999) 359–372.
[47] B. Aslibeiki, P. Kameli, H. Salamati, M. Eshraghi, T. Tahmasebi, Superspin glass state in $MnFe_2O_4$ nanoparticles, Journal of Magnetism and Magnetic Materials 322 (2010) 2929–2934.
[48] T. Hyeon, Y. Chung, J. Park, S.S. Lee, Y.W. Kim, B.H. Park, Synthesis of highly crystalline and monodisperse cobalt ferrite nanocrystals, Journal of Physical Chemistry B 106 (2002) 6831–6833.
[49] A.J. Rondinone, C. Liu, Z.J. Zhang, Determination of magnetic anisotropy distribution and anisotropy constant of manganese spinel ferrite nanoparticles, Journal of Physical Chemistry B 105 (2001) 7967–7971.